

# Photochemistry of Methyltrioxorhenium Revisited: A DFT/TD-DFT and CASSCF/MS-CASPT2 Theoretical Study

Paulo Jorge Costa,<sup>†,‡</sup> Maria José Calhorda,<sup>\*,†,‡</sup> Julien Bossert,<sup>§</sup> Chantal Daniel,<sup>\*,§</sup> and Carlos C. Romão<sup>‡</sup>

*Departamento de Química e Bioquímica, Faculdade de Ciências da Universidade de Lisboa, 1749-016 Lisboa, Portugal, Instituto de Tecnologia Química e Biológica (ITQB), Avenida da República, EAN, Apartado 127, 2781-901 Oeiras, Portugal, and Laboratoire de Chimie Quantique, UMR 7177 CNRS/ Université Louis Pasteur, Institut Le Bel, 4 Rue Blaise Pascal, 67 000 Strasbourg, France*

Received May 4, 2006

The electronic structure of (CH<sub>3</sub>)ReO<sub>3</sub> was reanalyzed by means of DFT calculations (ADF and Gaussian03 programs). TD-DFT calculations were carried out, using the DFT-optimized structure and several functionals, to assign the electronic excitations and interpret the dissociative behavior under irradiation. The agreement between calculated and experimental wavelengths was very good and could not be improved when using highly correlated methods (CASSCF/MS-CASPT2). The lowest energy transition at 260 nm was assigned to a LMCT from p O to Re d ( $\pi^*$  Re–O), correcting the earlier empirical assignment. The second transition, experimentally observed at 240 nm, is assigned to a charge transfer from C and O to Re in TD-DFT, but the weight of the C participation drops significantly in the CASSCF/MS-CASPT2 approach. (C<sub>2</sub>H<sub>5</sub>)ReO<sub>3</sub> exhibits a similar behavior. On the other hand, for (C<sub>6</sub>H<sub>5</sub>)ReO<sub>3</sub> and {C<sub>6</sub>H<sub>3</sub>(CH<sub>3</sub>)<sub>3</sub>}ReO<sub>3</sub> the strong low-energy absorption results from a LMCT from the phenyl  $\pi^*$  to d Re ( $\pi^*$  Re–O), reproducing the experimental trends.

## Introduction

The photochemistry of organometallic compounds has become an important field of chemistry, and the family of carbonyl derivatives, to which most initial studies were devoted,<sup>1</sup> was soon joined by other types of complexes characterized by the presence of metals in high formal oxidation states. Among many oxide derivatives, methyltrioxorhenium (MTO), (CH<sub>3</sub>)ReO<sub>3</sub>, has attracted much attention and has been the object of several studies.<sup>2</sup> This remarkable molecule catalyzes a wide number of reactions involving alkenes and alkynes, such as olefin metathesis, oxidation, and aldehyde olefination.<sup>3</sup> It displays different photochemical reactivity in solution<sup>4</sup> and in frozen matrix,<sup>5</sup> as has been shown recently. Instead of generating methyl radicals by Re–C bond homolysis, a carbene tautomer is formed in frozen matrix (although the tautomerization mechanism most likely proceeds through the formation of methyl and ReO<sub>3</sub> radicals), which may play a relevant role in olefin metathesis. Also recently, C–H···O interactions were detected for MTO

in the solid state.<sup>6</sup> Other related RReO<sub>3</sub> molecules are well known, but they differ in their behavior and properties, including catalytic and photochemical activity.<sup>7</sup> Several theoretical studies have addressed different aspects of the chemistry of MTO,<sup>8</sup> namely, the homolysis of the Re–C bond,<sup>9</sup> but to our knowledge, none have addressed the photochemistry of MTO and other trioxorhenium complexes by means of modern quantum-chemical calculations.

In this work, we analyze the UV–vis spectra and the photochemical reactivity of the (CH<sub>3</sub>)ReO<sub>3</sub> molecule, using TD-DFT methods (ADF<sup>10</sup> and Gaussian 03<sup>11</sup>) and highly correlated CASSCF and MS-CASPT2 approaches (MOLCAS<sup>12</sup>). The results from all the methods are discussed and compared with experimental data. The study was extended to species containing larger R groups than CH<sub>3</sub> (C<sub>2</sub>H<sub>5</sub>, C<sub>6</sub>H<sub>5</sub>, and C<sub>6</sub>H<sub>3</sub>(CH<sub>3</sub>)<sub>3</sub>).

\* Corresponding authors. E-mail: mjcalh@fc.ul.pt; daniel@quantix.u-strasbg.fr.

<sup>†</sup> Universidade de Lisboa.

<sup>‡</sup> ITQB.

<sup>§</sup> UMR 7177 CNRS/Université Louis Pasteur.

(1) Geoffroy, G. L.; Wrighton, M. S. *Organometallic Photochemistry*; Academic Press: New York, 1979.

(2) (a) Romão, C. C.; Kühn, F. E.; Herrmann, W. A. *Chem. Rev.* **1997**, *97*, 3197. (b) Herrmann, W. A. *J. Organomet. Chem.* **1995**, *500*, 149.

(3) (a) Kühn, F. E.; Scherbaum A.; Herrmann, W. A. *J. Organomet. Chem.* **2004**, *689*, 4149. (b) Jacob, J.; Espenson, J. H.; Jensen, J. H.; Gordon, M. S. *Organometallics* **1998**, *17*, 1835.

(4) (a) Herrmann, W. A.; Kühn, F. E.; Fiedler, D. A.; Mattner, M. R.; Geisberger, M. R.; Kunkeley, H.; Vogler, A.; Steenken, S. *Organometallics* **1995**, *14*, 5377. (b) Kunkeley, H.; Türk, T.; Teixeira, C.; Meric de Bellefon, C.; Herrmann, W. A.; Vogler, A. *Organometallics* **1991**, *10*, 2090.

(5) (a) Morris, L. J.; Downs, A. J.; Greene, T. M.; McGrady, G. S.; Herrmann, W. A.; Sirsch, P.; Gropen, O.; Scherer, W. *Chem. Commun.* **2000**, *67*. (b) Morris, L. J.; Downs, A. J.; Greene, T. M.; McGrady, G. S. *Organometallics* **2001**, *20*, 2344.

(6) Vaz, P. D.; Ribeiro-Claro, P. J. A. *Eur. J. Inorg. Chem.* **2005**, 1836

(7) (a) Downs, A. J.; Geisberger, M. R.; Green, J. C.; Greene, T. M.; Haaland, A.; Herrmann, W. A.; Morris, L. J.; Parsons, S.; Scherer, W.; Volden, H. V. *J. Chem. Soc., Dalton Trans.* **2002**, 3342. (b) Downs, A. J.; Dierker, G.; Green, J. C.; Greene, T. M.; McGrady, G. S.; Morris, L. J.; Scherer, W.; Sirsch, P. *J. Chem. Soc., Dalton Trans.* **2002**, 3349. (c) Morris, L. J.; Downs, A. J.; Green, J. C.; Greene, T. M.; Teat, S. J.; Parsons, S. *J. Chem. Soc., Dalton Trans.* **2002**, 3142. (d) Meric de Bellefon, C.; Herrmann, W. A.; Kiprof, P.; Whitaker, C. R. *Organometallics* **1992**, *11*, 1072.

(8) (a) di Valentin, C.; Gandolfi, R.; Gisdakis, P.; Rösch, N. *J. Am. Chem. Soc.* **2001**, *123*, 2365. (b) Gisdakis, P.; Yudanov, I. V.; Rosch, N. *Inorg. Chem.* **2001**, *40*, 3755. (c) Gisdakis, P.; Rösch, N.; Bencze, E.; Mink, J.; Gonçalves, I. S.; Kühn, F. E. *Eur. J. Inorg. Chem.* **2001**, 981. (d) Kostlmeier, S.; Haberlen, O. D.; Rosch, N.; Herrmann, W. A.; Solouki, B.; Bock, H. *Organometallics* **1996**, *15*, 1872.

(9) Mealli, C.; López, J. A.; Calhorda, M. J.; Romão, C. C.; Herrmann, W. A. *Inorg. Chem.* **1994**, *33*, 1139.

(10) (a) ADF2004.01, SCM, Theoretical Chemistry, Vrije Universiteit: Amsterdam, The Netherlands, <http://www.scm.com>. (b) te Velde, G.; Bickelhaupt, F. M.; van Gisbergen, S. J. A.; Guerra, C. F.; Baerends, E. J.; Snijders, J. G.; Ziegler, T. *J. Comput. Chem.* **2001**, *22*, 931. (c) Guerra, C. F.; Snijders, G.; te Velde, G.; Baerends, E. J. *Theor. Chem. Acc.* **1998**, *99*, 391.

### Computational Details

Density functional theory calculations<sup>13</sup> were carried out with the Amsterdam Density Functional program (ADF 2004.01)<sup>10</sup> and Gaussian03<sup>11</sup> packages. Within the ADF package, the local spin density (LSD) exchange correlation potential was used with the local density approximation of the correlation energy (Vosko, Wilk, and Nusair).<sup>14</sup> Gradient-corrected geometry optimizations<sup>15</sup> under  $C_{3v}$  symmetry were performed using the generalized gradient approximation (Perdew–Wang nonlocal exchange and correlation corrections, PW91).<sup>16</sup> A triple- $\zeta$  Slater-type orbital (STO) basis set augmented by two polarization functions was used for Re, O, C, and H. Relativistic effects were treated with the ZORA approximation.<sup>17</sup> A frozen core approximation was used to treat the core electrons: (1s) for C and O, ([1–4]s, [2–4]p, [3–4]d) for Re. Time-dependent DFT calculations (TD-DFT)<sup>18</sup> in the ADF implementation were used to determine the excitation energies asking for the lowest 10 singlet–singlet and singlet–triplet excitation energies on the PW91-optimized geometry. In the TD-DFT calculations, PW91, Becke exchange<sup>19</sup> plus Perdew correlation<sup>20</sup> (BP) GGA functionals, the shape-corrected XC functional of van Leeuwen and Baerends (LB94),<sup>21</sup> and the gradient-regulated asymptotic corrected potential GACLB<sup>22</sup> were used. The latter one requires the ionization potential of the molecule (experimental value 11.63 eV<sup>23</sup>).

Within Gaussian03, geometry optimizations were performed at the DFT/B3LYP<sup>24,25</sup> level using  $C_{3v}$  symmetry. This functional includes a mixture of Hartree–Fock exchange with DFT exchange–correlation, given by Becke’s three-parameter functional<sup>25</sup> with the Lee, Yang, and Parr correlation functional,<sup>24</sup> which includes both local and nonlocal terms. The standard LANL2DZ basis set was used with the associated ECP<sup>26</sup> for Re plus an f polarization function

(11) Frisch, M. J.; Trucks, G. W.; Schlegel, H. B.; Scuseria, G. E.; Robb, M. A.; Cheeseman, J. R.; Zakrzewski, V. G.; Montgomery, J. A., Jr.; Stratmann, R. E.; Burant, J. C.; Dapprich, S.; Millam, J. M.; Daniels, A. D.; Kudin, K. N.; Strain, M. C.; Farkas, O.; Tomasi, J.; Barone, V.; Cossi, M.; Cammi, R.; Mennucci, B.; Pomelli, C.; Adamo, C.; Clifford, S.; Ochterski, J.; Petersson, G. A.; Ayala, P. Y.; Cui, Q.; Morokuma, K.; Malick, D. K.; Rabuck, A. D.; Raghavachari, K.; Foresman, J. B.; Cioslowski, J.; Ortiz, J. V.; Stefanov, B. B.; Liu, G.; Liashenko, A.; Piskorz, P.; Komaromi, I.; Gomperts, R.; Martin, R. L.; Fox, D. J.; Keith, T.; Al-Laham, M. A.; Peng, C. Y.; Nanayakkara, A.; Gonzalez, C.; Challacombe, M.; Gill, P. M. W.; Johnson, B. G.; Chen, W.; Wong, M. W.; Andres, J. L.; Head-Gordon, M.; Replogle, E. S.; Pople, J. A. *Gaussian 03*, Revision B.04; Gaussian, Inc.: Pittsburgh, PA, 2003.

(12) Karlström, G.; Lindh, R.; Malmqvist, P.-Å.; Roos, B. O.; Ryde, U.; Veryazov, V.; Widmark, P.-O.; Cossi, M.; Schimmelpfennig, B.; Neogrady, P.; Seijo, L. *Comput. Mater. Sci.* **2003**, *28*, 222.

(13) Parr, R. G.; Yang, W. *Density Functional Theory of Atoms and Molecules*; Oxford University Press: New York, 1989.

(14) Vosko, S. H.; Wilk, L.; Nusair, M. *Can. J. Phys.* **1980**, *58*, 1200.

(15) (a) Versluis, L.; Ziegler, T. *J. Chem. Phys.* **1988**, *88*, 322. (b) Fan, L.; Ziegler, T. *J. Chem. Phys.* **1991**, *95*, 7401.

(16) Perdew, J. P.; Chevary, J. A.; Vosko, S. H.; Jackson, K. A.; Pederson, M. R.; Singh, D. J.; Fiolhais, C. *Phys. Rev. B* **1992**, *46*, 6671.

(17) van Lenthe, E.; Ehlers, A.; Baerends, E. J. *J. Chem. Phys.* **1999**, *110*, 8943.

(18) (a) van Gisbergen, S. J. A.; Groeneveld, J. A.; Rosa, A.; Snijders, J. G.; Baerends, E. J. *J. Phys. Chem.* **1999**, *103*, 3A, 6835. (b) Rosa, A.; Baerends, E. J.; van Gisbergen, S. J. A.; van Lenthe, E.; Groeneveld, J. A.; Snijders, J. G. *J. Am. Chem. Soc.* **1999**, *121*, 10356. (c) van Gisbergen, S. J. A.; Rosa, A.; Ricciardi, G.; E. Baerends, J. *J. Chem. Phys.* **1999**, *111*, 2499.

(19) Becke, A. D. *Phys. Rev. A* **1988**, *38*, 3098.

(20) Perdew, J. P. *Phys. Rev. B* **1986**, *33*, 8822.

(21) van Leeuwen, R.; Baerends, E. J. *Phys. Rev. A* **1994**, *49*, 2421.

(22) Grüning, M.; Gritsenko, O. V.; van Gisbergen, S. J. A.; Baerends, E. J. *J. Chem. Phys.* **2001**, *114*, 652.

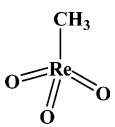
(23) Simone, M.; Coreno, M.; Green, J.; McGrady, S.; Pritchard, H. *Inorg. Chem.* **2003**, *42*, 1908.

(24) Lee, C.; Yang, W.; Parr, R. G. *Phys. Rev. B* **1988**, *37*, 785.

(25) Becke, A. D. *J. Chem. Phys.* **1993**, *98*, 5648.

(26) (a) Hay, P. J.; Wadt, W. R. *J. Chem. Phys.* **1985**, *82*, 270. (b) Wadt, W. R.; Hay, P. J. *J. Chem. Phys.* **1985**, *82*, 284. (c) Hay, P. J.; Wadt, W. R. *J. Chem. Phys.* **1985**, *82*, 299.

**Table 1. Distances (Å) and Angles (deg) in MTO**



	ED <sup>34</sup>	neutron <sup>a 35</sup>	ADF (PW91)	G03 (B3LYP)
Re–C	2.060	2.063	2.098	2.069
Re–O	1.709	1.702	1.715	1.693
C–Re–O	106	106	107	105
O–Re–O	113	113	113	112
H–C–Re	112	108	109	109

<sup>a</sup> (CD<sub>3</sub>)ReO<sub>3</sub>.

(0.869).<sup>27</sup> The 6-311G\*\* basis set<sup>28</sup> was used for the other atoms (C, O, H). TD-DFT calculations were also performed using the Gaussian03 implementation<sup>29</sup> on the B3LYP-optimized structure.

The CASSCF/MS-CASPT2 calculations were performed using MOLCAS<sup>12</sup> on the B3LYP-optimized structure. The CASSCF calculations were performed correlating 14 electrons in 10 active orbitals. Averaged CASSCF calculations over 6 roots keeping  $C_{3v}$  symmetry, using supersymmetry and cleaning orbital coefficients, were performed for a given spin. The CASSCF wave functions were used as references in subsequent CASPT2 calculations using the *level shift* corrected perturbation method<sup>30</sup> with a value of 0.3. The Re atom was described by the Dolg ECP ( $Z = 15.0$ ) with an associated (8s,7p,6d) valence basis set.<sup>31</sup> The following atomic natural orbitals (ANO)<sup>32</sup> basis sets have been used for the C, O, and H atoms in the all-electron scheme: for the C and O atoms a (10s, 6p, 3d) set contracted to [4s, 3p, 2d]; for the H atoms a (7s, 3p) set contracted to [3s, 2p].

The solvent effects were included using the Conductor-like Screening Model (COSMO)<sup>33</sup> implemented in ADF.

### Results and Discussion

**MTO: Geometry and Properties.** The geometry of MTO is well known, having been determined in the gas phase by electron diffraction (ED in Table 1).<sup>34</sup> MTO decomposes under the X-ray irradiation at low temperatures. Single-crystal diffraction data are available for the deuterated analogue, (CD<sub>3</sub>)-ReO<sub>3</sub> (neutron column in Table 1), or for the MTO polymer.<sup>35</sup> The geometry was fully optimized, under  $C_{3v}$  symmetry, by means of DFT calculations,<sup>13</sup> using both ADF<sup>10</sup> and Gaussian03<sup>11</sup> (see Computational Details). In the ADF calculation, it

(27) Ehlers, A. W.; Böhme, M.; Dapprich, S.; Gobbi, A.; Höllwarth, A.; Jonas, V.; Köhler, K. F.; Stegmann, R.; Veldkamp, A.; Frenking, G. *Chem. Phys. Lett.* **1993**, *208*, 111.

(28) (a) McLean, A. D.; Chandler, G. S. *J. Chem. Phys.* **1980**, *72*, 5639. (b) Krishnan, R.; Binkley, J. S.; Seeger, R.; Pople, J. A. *J. Chem. Phys.* **1980**, *72*, 650.

(29) (a) Stratmann, R. E.; Scuseria, G. E.; Frisch, M. J. *J. Chem. Phys.* **1998**, *109*, 8218. (b) Bauernschmitt, R.; Ahlrichs, R. *Chem. Phys. Lett.* **1996**, *256*, 454. (c) Casida, M. E.; Jamorski, C.; Casida, K. C.; Salahub, D. R. *J. Chem. Phys.* **1998**, *108*, 4439.

(30) Roos, B. O.; Andersson, K.; Fülcher, M. P.; Serrano-Andrés, L.; Pierloot, K.; Merchán, M.; Molina, V. *THEOCHEM* **1996**, *388*, 257.

(31) Andrae, D.; Haeussermann, U.; Dolg, M.; Stoll, H.; Preuss, H. *Theor. Chim. Acta* **1990**, *77*, 123.

(32) Pierloot, K.; Dumez, B.; Widmark, P. O.; Roos, B. O. *Theor. Chim. Acta* **1995**, *90*, 87.

(33) (a) Klamt, A.; Schüürmann, G. *J. Chem. Soc., Perkin Trans.* **1993**, *2*, 799. (b) Klamt, A. *J. Phys. Chem.* **1995**, *99*, 2224. (c) Klamt, A.; Jones, V. *J. Chem. Phys.* **1996**, *105*, 9972. (c) Pye, C. C.; Ziegler, T. *Theor. Chem. Acc.* **1999**, *101*, 396.

(34) Herrmann, W. A.; Kiprof, P.; Rypdal, K.; Tremmel, J.; Blom, R.; Alberto, R.; Behm, J.; Albach, R. W.; Bock, H.; Soulouki, B.; Mink, J.; Lichtenberger, D.; Gruhn, N. E. *J. Am. Chem. Soc.* **1991**, *113*, 6257.

(35) Herrmann, W. A.; Scherer, W.; Fischer, R. W.; Blümel, J.; Kleine, M.; Mertin, W.; Gruehn, R.; Mink, J.; Boysen, H.; Wilson, C. C.; Ibberson, R. M.; Bachmann, L.; Mattner, M. *J. Am. Chem. Soc.* **1995**, *117*, 3231.

**Table 2. Calculated (G03, ADF) and Experimental IR Frequencies**

symmetry	calculated		experimental			assignment
	ADF (PW91)	G03 (B3LYP)	Ar matrix <sup>5</sup>	C <sub>6</sub> H <sub>6</sub> solution <sup>34</sup>	CCl <sub>4</sub> solution <sup>36</sup>	
A <sub>2</sub>	189	171			230	CH <sub>3</sub> torsion
A <sub>1</sub>	265	258	324		235	$\delta$ ReO <sub>3</sub> s
	565	563	565	575	567	$\nu$ Re–C
E	1003	1050	1001	998	1000	$\nu$ Re–O s
	1194	1249	1210	1205	1205	$\delta$ CH <sub>3</sub> s
	2975	3037	2926	2899	2909	$\nu$ C–H s
	208	213			248	$\delta$ ReCO a
	325	329	253		262	$\rho$ ReO <sub>3</sub> a
E	715	757	735	739	736	$\rho$ CH <sub>3</sub>
	974	1011	970	947	965	$\nu$ Re–O a
	1378	1428	1377	1363	1372	$\delta$ CH <sub>3</sub> a
	3069	3134	3013	2989	2994	$\nu$ C–H a

was checked that the staggered conformation was stabilized, relative to the eclipsed one, by 2 kcal mol<sup>-1</sup>.

The agreement with the experimental structure is good in the two cases, for both the distances and the angles, as can be seen from the data in Table 1 and as has been reported in previous calculations performed on the same molecule.<sup>8</sup> The largest, though small, deviations are found for the H–C–Re angle.

Since the G03/B3LYP geometry is slightly better, namely, the Re–C bond length (2.069 Å), which is closer to the experimental one (2.060 Å), than the ADF value (2.098 Å), we subsequently used it in all CASSCF calculations.

In MTO, rhenium is formally d<sup>0</sup>. The metal is more electron rich than it may seem, as the oxide ligands are  $\pi$ -donors and thereby contribute to increase the electronic density at the rhenium. A qualitative bonding picture shows the  $\sigma$ - and  $\pi$ -donation from the oxides and  $\sigma$ -donation from the methyl group to the metal, as has been described in detail in an earlier publication.<sup>9</sup>

The quality of the computational approach was checked by the calculation of some other properties of MTO, namely, the IR spectra (G03 and ADF). There is a good agreement between the calculated and the experimental values, as can be seen in Table 2.

One should notice that these values are not scaled. The application of a scaling factor would lead to a better numerical agreement. The major discrepancy observed in the assignments concerns the two lowest energy asymmetric vibrational modes,  $\delta$  ReCO and  $\rho$  ReO<sub>3</sub>.

**Frontier Orbitals.** The frontier orbitals of MTO are depicted in Figure 1, and their composition and character are shown in Table 3, as calculated with the PW91 functional (ADF). The DFT calculations with different functionals yield very similar results concerning the MO compositions (see Tables SI-1 to SI-4 in the Supporting Information) and their relative positions. MO levels with the same composition follow the same order. The HOMO–LUMO gap obtained with the hybrid B3LYP functional (6.14 eV), however, is considerably larger than the HOMO–LUMO gaps obtained with the GGA functionals (ca. 4 eV). As expected from a d<sup>0</sup> species, the LUMOs are essentially Re d orbitals, while the HOMOs consist of combinations of oxygen lone pairs, followed, at lower energies, by  $\sigma$ -bonding Re–C levels, mostly localized on the methyl group.

The HOMO is the antibonding combination of p lone pairs from the three oxygen atoms (2a<sub>2</sub>). It remains Re–O nonbonding, since there is no d Re orbital of suitable symmetry to interact with it. Immediately below comes the 8e pair, consisting mainly of oxygen p lone pairs (two bonding and one antibonding interactions), with a small antibonding contribution of Re p (x

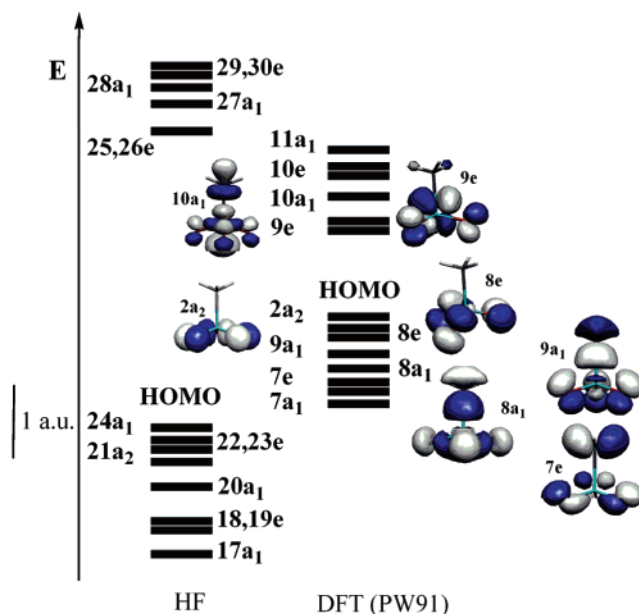


**Figure 1.** Energy of the frontier orbitals of MTO, calculated using HF (G03) (left) and PW91 (ADF) (right), as well as representation of the PW91 orbitals (only one of each degenerate orbitals of e symmetry).

or y) orbitals. The Re p<sub>z</sub> participates in an antibonding interaction with in-phase combination of the oxygen p<sub>z</sub> orbital and the methyl lone pair in orbital 9a<sub>1</sub>, which is mainly p O, p C in character ( $\sigma^*$  Re–C concerning Re–C interaction). The other occupied relevant orbital of a<sub>1</sub> symmetry is 8a<sub>1</sub>. This is a  $\sigma$  Re–C and Re–O bonding orbital, mostly localized in the ligands (also p O, p C), with Re d<sub>z<sup>2</sup></sub> and high 6s character. The 7e set is mainly a  $\pi$  Re–O orbital with significant contribution of the methyl ( $\pi^*$  Re–C). In the unoccupied orbitals, Re d contributes mostly to 10a<sub>1</sub> (which is  $\pi$  antibonding toward oxygen and  $\sigma$  antibonding to the methyl carbon) and to 9e, which is  $\pi^*$  Re–O.

We also calculated the energy levels at the Hartree–Fock level of theory (see Figure 1). The results are different from the ones obtained at the DFT level of theory regarding the relative order of the orbitals. In the HF calculations, the HOMO is 24a<sub>1</sub> (equivalent to 9a<sub>1</sub> in PW91), while the a<sub>2</sub> orbital is only HOMO–3. These changes in the occupied orbitals, as well as some changes in the virtual ones, could lead to wrong assignments of the absorption spectra based on qualitative MO diagrams in which the MOs have a different order (vide infra). The same was already shown for the assignment of PES spectra.<sup>8d</sup>

**TD-DFT Calculations and UV–Vis Spectra.** The summary of the results for the PW91 calculations (ADF), including some experimental data for comparison, is given in Table 4. For detailed information, see Table SI-5 in the Supporting Information.

The experimental electronic spectra of MTO in *n*-hexane consist of three absorption bands, with maxima at 260, 231, and 205 nm.<sup>4b</sup> These maxima are solvent dependent and should correspond to LMCT since no MC or MLCT are available (Re is formally d<sup>0</sup>).

Our TD-DFT gas-phase results show three sets of electronic transitions. The first, centered on the b<sup>1</sup>A<sub>1</sub> state (also involving a<sup>1</sup>E and b<sup>1</sup>E states) should correspond to the experimentally observed band at 260 nm. The wavelength used for irradiation in many experiments (254 nm)<sup>4a,5</sup> where Re–C bond homolysis is observed corresponds to this transition energy. All these

**Table 3. Nature, Energies (eV), and Main Compositions (%) of the Relevant Frontier Orbitals of MTO (ADF–PW91)**

orbital	E (eV)	symmetry	composition (%)			character
			Re	O	C	
LUMO+2	-1.985	10a <sub>1</sub>	42 d <sub>z<sup>2</sup></sub> , 6 p <sub>z</sub>	20 p <sub>z</sub>	23 p <sub>z</sub>	d Re( $\sigma^*$ Re–C)
LUMO <sup>a</sup>	-3.932	9e	47 d <sub>yz</sub> , 3 d <sub>xy</sub>	23 p <sub>z</sub> , 10 p <sub>x</sub> , 7 p <sub>y</sub>		d Re( $\pi^*$ Re–O)
HOMO	-8.089	2a <sub>2</sub>		97 p <sub>y</sub>		p O lone pairs
HOMO–1 <sup>a</sup>	-8.409	8e	2 p <sub>x</sub>	45 p <sub>z</sub> , 41 p <sub>x</sub>		p O lone pairs
HOMO–3	-8.716	9a <sub>1</sub>	6 p <sub>z</sub>	42 p <sub>z</sub> , 18 p <sub>x</sub>	22 p <sub>z</sub>	p O, p C ( $\sigma^*$ Re–C)
HOMO–4	-9.827	8a <sub>1</sub>	5 d <sub>z<sup>2</sup></sub> , 9 s	54 p <sub>x</sub>	19 p <sub>z</sub>	p O, p C ( $\sigma$ Re–C)
HOMO–5 <sup>a</sup>	-10.319	7e	16 d <sub>yz</sub>	27 p <sub>x</sub> , 12 p <sub>z</sub>	15 p <sub>y</sub>	d Re, p O, p C ( $\pi$ Re–O, $\pi^*$ Re–C)

<sup>a</sup> Only one set of the e orbitals.

**Table 4. Calculated (PW91) Excitation Energies (eV, nm), Oscillator Strengths (*f*), Composition ( $\omega$ ), and Nature of the Transitions for MTO (the A<sub>2</sub> states are omitted), in the Gas-Phase and in *n*-Hexane (COSMO model)**

state	E/eV	E/nm	f	one-electron excitation in the main configuration	$\omega$ (%)	$\lambda_{\max}^{4b}$	
Gas-Phase							
a <sup>1</sup> E	2a <sub>2</sub> → 9e	4.34685	285	0.0025	p O → d Re ( $\pi^*$ Re–O)	94.4	
b <sup>1</sup> E	8e → 9e	4.65267	266	0.0036	p O → d Re ( $\pi^*$ Re–O)	74.6	
	9a <sub>1</sub> → 9e				p O, p C ( $\sigma^*$ Re–C) → d Re ( $\pi^*$ Re–O)	21.3	
b <sup>1</sup> A <sub>1</sub>	8e → 9e	4.72109	262	0.0054	p O → d Re ( $\pi^*$ Re–O)	99.4	260
c <sup>1</sup> E	9a <sub>1</sub> → 9e	5.30887	234	0.0063	p O, p C ( $\sigma^*$ Re–C) → d Re ( $\pi^*$ Re–O)	70.9	
	8e → 9e				p O → d Re ( $\pi^*$ Re–O)	14.9	
d <sup>1</sup> E	8a <sub>1</sub> → 9e	6.14128	202	0.0037	p O, p C ( $\sigma$ Re–C) → d Re ( $\pi^*$ Re–O)	90.1	205
Solvent ( <i>n</i> -hexane)							
a <sup>1</sup> E	2a <sub>2</sub> → 9e	4.5021	275	0.0024	p O → d Re ( $\pi^*$ Re–O)	92.2	
b <sup>1</sup> E	8e → 9e	4.7248	262	0.0021	p O → d Re ( $\pi^*$ Re–O)	49.3	
	9a <sub>1</sub> → 9e				p O, p C ( $\sigma^*$ Re–C) → d Re ( $\pi^*$ Re–O)	47.3	
b <sup>1</sup> A <sub>1</sub>	8e → 9e	4.8714	255	0.0055	p O → d Re ( $\pi^*$ Re–O)	99.3	260
c <sup>1</sup> E	9a <sub>1</sub> → 9e	5.2302	237	0.0088	p O, p C ( $\sigma^*$ Re–C) → d Re ( $\pi^*$ Re–O)	46.8	
	8e → 9e				p O → d Re ( $\pi^*$ Re–O)	35.6	
d <sup>1</sup> E	8a <sub>1</sub> → 9e	6.0867	204	0.0045	p O, p C ( $\sigma$ Re–C) → d Re ( $\pi^*$ Re–O)	73.2	
	7e → 9e				$\pi$ Re–O, $\pi^*$ Re–C → d Re ( $\pi^*$ Re–O)	20.1	

transitions correspond to excitations to the LUMO (9e), which is mainly Re d in character ( $\pi^*$  concerning Re–O interaction), starting from several of the highest occupied levels, which are characterized as oxygen lone pairs, with a small contribution (21%) from the 9a<sub>1</sub> orbital. This allows us to assign the observed maxima at 260 nm to a LMCT p O → d Re ( $\pi^*$  Re–O) transition. This assignment is in agreement with the vibrational progression of this absorption, but disagrees with the previous assignment made in the literature ( $\sigma$  Re–C →  $\pi^*$  Re–O).<sup>4b</sup> This previous assignment assumed that the lowest energy band was originated from the HOMO, which based on qualitative MO diagrams was the a<sub>1</sub> symmetry orbital, corresponding to the Re–C  $\sigma$  bonding interaction.

The second set corresponds to the c<sup>1</sup>E state and is responsible for the observed band at 231 nm. This transition is assigned to a LMCT from C and O p centered orbitals to the Re d orbitals ( $\pi^*$  Re–O). The last set, with d<sup>1</sup>E and remaining higher states (not shown), corresponds to the observed maxima at 205 nm, which are also assigned to a LMCT.

Since the energies and assignments of transitions are in many cases very sensitive to the presence of solvent,<sup>37</sup> we also performed TD-DFT calculations using the COSMO solvation model to mimic the *n*-hexane solvent used in the UV–vis experimental measurements. The results, also given in Table 4, do not significantly differ from the gas-phase ones. The first set of excitations is also centered on the b<sup>1</sup>A<sub>1</sub> at 255 nm and corresponds to a LMCT p O → d Re ( $\pi^*$  Re–O) transition. A small change occurs in the b<sup>1</sup>E state, where the 9a<sub>1</sub> → 9e contribution, which involves the Re–C level, becomes more

important. The calculated oscillator strength is very similar for gas phase (0.0054) and *n*-hexane (0.0055). The next maximum is calculated at 237 nm and corresponds to the observed band at 231 nm (234 nm in the gas phase). The weight of the 9a<sub>1</sub> → 9e transition is now much smaller than in the gas phase, but this excitation can still be assigned as a LMCT from C and O p centered orbitals to the Re d orbitals ( $\pi^*$  Re–O). The calculated oscillator strength (0.0088) is higher than the one calculated in the gas phase (0.0066) for this transition. The last set is also composed of the d<sup>1</sup>E and remaining higher states (not shown). This transition has slightly higher oscillator strength in *n*-hexane, and the character is essentially the same.

The calculations in the gas phase and solvent provide essentially the same results, the agreement with experimental values being even better for the gas-phase calculation, especially if we consider the two lowest energy bands. The PW91-calculated oscillator strengths provide the correct intensity of the two lowest experimental bands but give a value that is too low for the experimental 205 nm. Nevertheless, since the main interest is on the lowest energy bands and the TD-DFT (PW91) gas-phase calculations are in excellent agreement with the experiment, all the subsequent calculations will refer to the gas phase.

We also performed TD-DFT calculations using ADF and other functionals (GRAC, BP, LB94) besides PW91, as well as B3LYP in Gaussian03, to test the stability and the functional dependence of the TD-DFT calculations. Summarized results are shown in Table 5. For detailed information, see Tables SI-6 to SI-9 in the Supporting Information.

The results obtained for PW91, BP, and GRAC are very similar, concerning the energies, oscillator strengths, and nature of the transitions. The GRAC functional is an asymptotic corrected potential, but no substantial changes are observed in

(36) Mink, J.; Keresztury, G.; Stirling, A.; Herrmann, W. A. *Spectrochim. Acta* **1994**, *50A*, 2039.

(37) (a) Vlček, A., Jr.; Zálšíš, S. *J. Phys. Chem. A* **2005**, *109*, 2991. (b) Fantacci, S.; Angelis, F.; Selloni, A. *J. Am. Chem. Soc.* **2003**, *125*, 4381.

**Table 5. Summary of the TD-DFT Lowest Excitation Energies (nm), Oscillator Strengths ( $f$ ), and Nature of the Low-Lying Electronic Transitions for MTO**

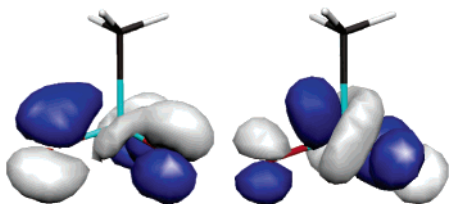
state	main character	energy ( $f$ )			main character	energy ( $f$ )		$\lambda_{\max}^{4b}$
		PW91	GRAC	BP		B3LYP	LB94	
a <sup>1</sup> E	p O $\rightarrow$ d Re ( $\pi^*$ Re–O)	285 (0.0025)	285 (0.0021)	285 (0.0023)	p O $\rightarrow$ d Re ( $\pi^*$ Re–O)	277 (0.0001)	304 (0.0018)	
b <sup>1</sup> E	p O $\rightarrow$ d Re ( $\pi^*$ Re–O)	266 (0.0036)	266 (0.0036)	267 (0.0036)	p O, p C $\rightarrow$ d Re ( $\pi^*$ Re–O)	249 (0.0023)	291 (0.0019)	
b <sup>1</sup> A <sub>1</sub>	p O $\rightarrow$ d Re ( $\pi^*$ Re–O)	262 (0.0054)	263 (0.0052)	263 (0.0044)	p O $\rightarrow$ d Re ( $\pi^*$ Re–O)	254 (0.0074)	283 (0.0032)	260
c <sup>1</sup> E	p O, p C $\rightarrow$ d Re ( $\pi^*$ Re–O)	234 (0.0063)	234 (0.0061)	234 (0.0061)	p O, p C $\rightarrow$ d Re ( $\pi^*$ Re–O)	224 (0.0067)	261 (0.0058)	231
d <sup>1</sup> E	p O, p C $\rightarrow$ d Re ( $\pi^*$ Re–O)	202 (0.0037)	202 (0.0037)	202 (0.0037)	p O, p C $\rightarrow$ d Re ( $\pi^*$ Re–O)	197 (0.0094)	221 (0.0042)	205

**Table 6. Calculated (CASSCF/MS-CASPT2) Excitation Energies (eV, nm), Oscillator Strengths ( $f$ ), Composition ( $\omega$ ), and Nature of the Transitions for MTO**

state		$E/eV$	$E/nm$	$f$	one-electron excitation in the main configuration	$\omega$ (%)	$\lambda_{\max}^{4b}$
b <sup>1</sup> A <sub>1</sub>	15a' $\rightarrow$ 17a'	4.81	257	0.0066	p O $\rightarrow$ d Re ( $\pi^*$ Re–O)	44.1	260
	7a'' $\rightarrow$ 9a''						
c <sup>1</sup> E	16a' $\rightarrow$ 17a'	5.16	240	0.0059	p O, d Re $\rightarrow$ d Re ( $\pi^*$ Re–O)	43.6	231
	7a'' $\rightarrow$ 9a''						
d <sup>1</sup> E	15a' $\rightarrow$ 18a'	5.84	212	0.0320	p O $\rightarrow$ d Re ( $\sigma^*$ Re–C)	40.4	205
	16a' $\rightarrow$ 17a'				p O d Re $\rightarrow$ d Re ( $\pi^*$ Re–O)	12.7	

these results, and all three give excellent agreement with the experimental values. The use of the hybrid functional B3LYP (Gaussian03) introduces some changes; for instance, the b<sup>1</sup>A<sub>1</sub> state is lower in energy than b<sup>1</sup>E. Another change is the character of the b<sup>1</sup>E transition, also observed for the LB94 functional, in which the participation of the methyl group becomes more important. The excitation is no longer mainly from the oxygen lone pairs, but a mixture of the p O, p C ( $\sigma^*$  Re–C) orbital. Also, the excitation calculated to appear at 285 nm with BP, GRAC, and PW91 functionals is obtained at 277 nm in the calculations with the hybrid B3LYP, but the oscillator strength is close to zero (0.0001). Since the experimental band at 260 nm is broad, it is likely that the excitations at 285 nm calculated with the GGA functionals also contribute to the broadening of this band. We shall come back to this point when discussing the CAS calculations (see below). In general, however, all functionals performed quite well since the agreement between the experimental and calculated energies is very good. The LB94 functional seems to be the worst in this case.

**CAS Calculations.** We performed CASSCF/MS-CASPT2 calculations in order to compare the values with the TD-DFT ones. The calculated transition energies of the low-lying singlet excited states of MTO are reported in Table 6. The values are also in excellent agreement with the experiment and with the ones obtained at the TD-DFT level of theory. The absorption observed experimentally at 260 nm is calculated at 257 nm and corresponds to a charge transfer from the oxygen lone pairs to a metal d centered orbital ( $\pi^*$  Re–O), in agreement with the assignment made by the TD-DFT results, thus confirming that the empirical assignment of this transition as a  $\sigma$  Re–C  $\rightarrow$   $\pi^*$  Re–O excitation<sup>4b</sup> was wrong. The orbitals involved in the calculated transition are depicted in Figure 2. Only the 15a' and 17a' are represented. The 7a'' and 9a'' orbitals are similar and correspond to the second element of the E set in C<sub>3v</sub> symmetry.

**Figure 2.** Representation of the molecular orbitals (15a' left, 17a' right) corresponding to the one-electron excitation responsible for the 254 nm transition calculated for MTO (CASSCF/MS-CASPT2).

They are all very similar to the Kohn–Sham orbitals 8e and 9e depicted in Figure 1.

Some differences are however observed for the calculated excitation at 240 nm. The TD-DFT calculations suggest that this transition has significant participation of the methyl group, being p O, p C  $\rightarrow$  d Re ( $\pi^*$  Re–O) in nature. The MS-CASPT2 calculations show that the methyl participation is overestimated and the Re participation is underestimated. The transition is mainly p O, d Re  $\rightarrow$  d Re ( $\pi^*$  Re–O).

CASSCF/MS-CASPT2 results show an excitation at 287 nm (not shown in Table 6), with a very small oscillator strength (0.0003), which compares very well with the B3LYP result (277 nm, 0.0001). All the other TD-DFT calculations (BP, GRAC, and PW91) led to a value of 285 nm with non-negligible oscillator strengths. Despite the very good results given by BP, GRAC, and PW91 functionals, the hybrid B3LYP functional provides a better agreement with both the experimental UV–vis spectra and the CASSCF/MS-CASPT2 calculations.

**Homolysis of the Re–C Bond.** DFT calculations (PW91), starting from the fully optimized geometry, were performed at several Re–C distances, and the evolution of the energy of each orbital was followed, as is shown in the Walsh diagram of Figure 3.

As the Re–C distance is increased, the 10a<sub>1</sub> orbital, which was  $\sigma^*_{\text{Re–C}}$  in character (see Table 3), is stabilized, by loss of the Re–C antibonding character. On the other hand, the energy of 9a<sub>1</sub> increases. This result is apparently anomalous, as this orbital was classified as Re–C antibonding. However, as the Re–C distance becomes longer, 9a<sub>1</sub> loses its Re p character, responsible for the antibonding nature, becoming more d( $z^2$ ) in character and bonding. This may be seen as mixing of several a<sub>1</sub> levels (8a<sub>1</sub> starts as a  $sd_z^2$  hybrid, Re–C bonding, though mostly localized in the ligands; 10a<sub>1</sub> is a d level). As 10a<sub>1</sub> is stabilized along the reaction coordinate, it loses d character.

It is interesting to notice that this diagram very closely matches the qualitative diagram obtained from extended Hückel calculations in an earlier calculation.<sup>9</sup> These results are insufficient to extract definitive conclusions about the dynamics of the photoprocess, but can, nevertheless, indicate the importance of the  $\sigma/\sigma^*_{\text{Re–C}}$  levels on the excitations when the Re–C bond is stretched.

**Other Related Molecules RReO<sub>3</sub> (R = C<sub>2</sub>H<sub>5</sub>, C<sub>6</sub>H<sub>5</sub>, C<sub>6</sub>H<sub>3</sub>–(CH<sub>3</sub>)<sub>3</sub>).** Since the TD-DFT results were satisfactory for MTO, we also performed TD-DFT (PW91) calculations on related species containing larger R groups (R = C<sub>2</sub>H<sub>5</sub>, C<sub>6</sub>H<sub>5</sub>, and C<sub>6</sub>H<sub>3</sub>–

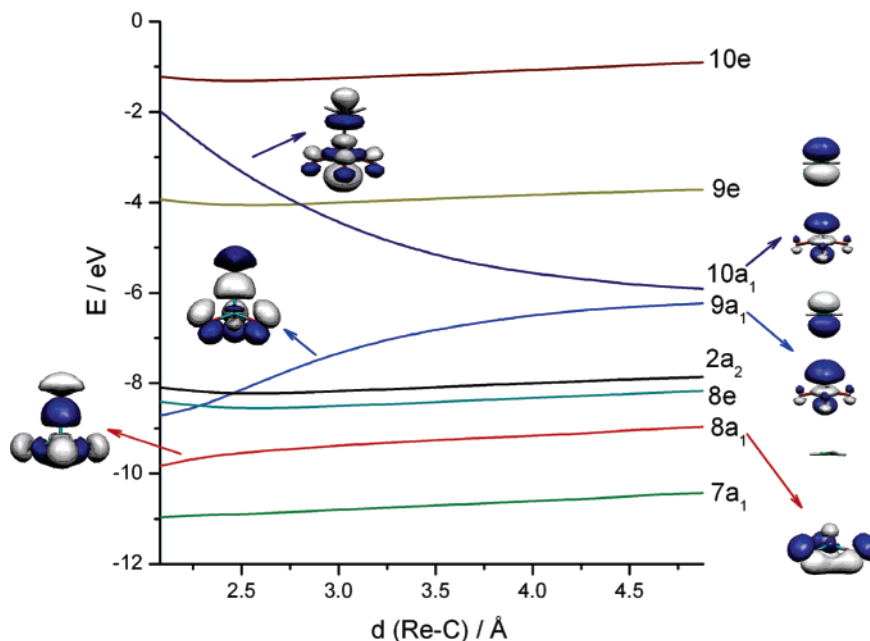


**Figure 3.** Walsh diagram for the evolution of the frontier orbitals of MTO, as the Re–C distance is stretched. Orbitals 10a<sub>1</sub>, 9a<sub>1</sub>, and 8a<sub>1</sub> are represented at Re–C distances of 2.02 Å (left) and 4.88 Å (right).

**Table 7.** Calculated (PW91) Excitation Energies (eV, nm), Oscillator Strengths (*f*), and Nature of the Transitions for RReO<sub>3</sub>

state	<i>E</i> /eV	<i>E</i> /nm	<i>f</i>	one-electron excitation in the main configuration	$\lambda_{\max}^{4a}$
R = C <sub>2</sub> H <sub>5</sub>					
a <sup>1</sup> A''	4.28	289	0.0022	p O → d Re (π* Re–O)	262
b <sup>1</sup> A'	4.33	286	0.0022	p O → d Re (π* Re–O)	
c <sup>1</sup> A'	4.41	281	0.0020	pO, pC → d Re (π*Re–O)	
d <sup>1</sup> A''	4.83	257	0.0056	pO, pC → d Re (π*Re–O)	
e <sup>1</sup> A'	4.86	255	0.0046	p O → d Re (π* Re–O)	
f <sup>1</sup> A'	5.67	218	0.0047	π* C–C → d Re (π* Re–O)	210
R = C <sub>6</sub> H <sub>5</sub>					
c <sup>1</sup> A'	3.86	321	0.1566	π Ph → d Re (π* Re–O)	334 <sup>a</sup>
R = C <sub>6</sub> H <sub>3</sub> (CH <sub>3</sub> ) <sub>3</sub>					
c <sup>1</sup> A'	3.56	348	0.1726	π Ph → d Re (π* Re–O)	334

<sup>a</sup> Value for C<sub>6</sub>H<sub>3</sub>(CH<sub>3</sub>)<sub>3</sub>.

(CH<sub>3</sub>)<sub>3</sub>). All of them exhibit the same behavior as MTO, namely, Re–C homolytic cleavage upon irradiation.<sup>4a</sup> Table 7 shows the summary of TD-DFT results on the PW91-optimized geometries using C<sub>s</sub> symmetry (detailed information can be found in Tables SI-9 to SI-11 in the Supporting Information).

Complex (C<sub>2</sub>H<sub>5</sub>)ReO<sub>3</sub> shows a behavior similar to that of MTO. Three UV–vis bands were reported, centered at 262, 240, and 210 nm in CH<sub>3</sub>CN.<sup>4b</sup> The TD-DFT results also show three sets of excitations. The first is centered at 286 nm (b<sup>1</sup>A') and corresponds to a LMCT from the oxygen lone pairs to a Re d orbital (π\* concerning Re–O interaction). The other excitations of the first set, calculated at 289 and 281 nm, should also contribute to the observed maxima at 262 nm and are also assigned as LMCT. Like for MTO, these results contradict the previous assignments made for this band as a σ Re–C → d Re transition.<sup>4b</sup>

The second maximum is centered at 257 nm, which compares quite well with the experimental value (240 nm) and corresponds to a LMCT from p O, p C to d Re (π\* Re–O). Finally, the observed band at 210 nm, calculated at 218 nm, is assigned to a LMCT from π\* orbitals on the C<sub>2</sub>H<sub>5</sub> to the d Re orbital (π\* Re–O).

For complex (C<sub>6</sub>H<sub>5</sub>)ReO<sub>3</sub>, no experimental UV–vis results are available. However, for the related complex {C<sub>6</sub>H<sub>3</sub>(CH<sub>3</sub>)<sub>3</sub>}-

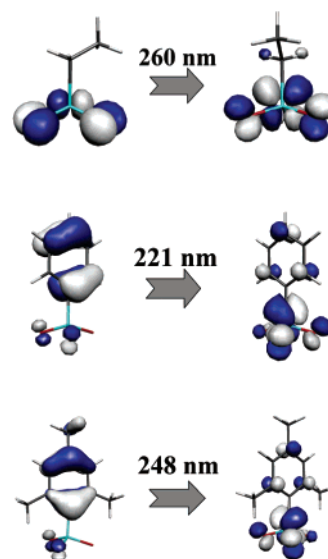


**Figure 4.** Representation of the orbitals corresponding to the excitations responsible for the Re–C homolytic cleavage for complexes (C<sub>2</sub>H<sub>5</sub>)ReO<sub>3</sub> (top), (C<sub>6</sub>H<sub>5</sub>)ReO<sub>3</sub> (center), and {C<sub>6</sub>H<sub>3</sub>(CH<sub>3</sub>)<sub>3</sub>}ReO<sub>3</sub> (bottom).

ReO<sub>3</sub>, one absorption band with a maximum at 334 nm was measured in CH<sub>3</sub>CN, and irradiation at 333 nm induces photolysis.<sup>4b</sup> The TD-DFT results show the same behavior for (C<sub>6</sub>H<sub>5</sub>)ReO<sub>3</sub> and {C<sub>6</sub>H<sub>3</sub>(CH<sub>3</sub>)<sub>3</sub>}ReO<sub>3</sub>. One intense peak is calculated at 321 and 348 nm, respectively, corresponding to a LMCT from π orbitals on the phenyl ring to a d Re orbital (π\* concerning Re–O interaction). This situation is very different from the previous complexes where the R group (R = CH<sub>3</sub> and C<sub>2</sub>H<sub>5</sub>) was not involved in the lowest energy excitations corresponding to the wavelength used for irradiation.

The orbitals involved in the lowest energy excitations responsible for the Re–C homolytic cleavage for complexes (C<sub>2</sub>H<sub>5</sub>)ReO<sub>3</sub>, (C<sub>6</sub>H<sub>5</sub>)ReO<sub>3</sub>, and {C<sub>6</sub>H<sub>3</sub>(CH<sub>3</sub>)<sub>3</sub>}ReO<sub>3</sub> are depicted in Figure 4.

### Conclusions

DFT calculations (ADF and Gaussian03 programs) were used to optimize the geometry of  $(\text{CH}_3)_3\text{ReO}_3$  and describe the electronic structure. TD-DFT (PW91) calculations carried out on the optimized structures led to a description of the excitation energies in close agreement to the experimental data. The lowest energy transition at 260 nm was assigned to a LMCT from p O to Re d ( $\pi^*$  Re–O), correcting the earlier empirical assignment as  $\sigma$  Re–C to  $\pi^*$  Re–O. The second transition, experimentally observed at 240 nm, is assigned to a charge transfer from C and O to Re, as well as the third one (231 nm). Other functionals were tested (BP, GRAC, LB94, B3LYP), with only minor changes in outcome. The excitation energies obtained from highly correlated methods (CASSCF/MS-CASPT2) were very similar, the only significant difference being the nature of the second transition, which lost the C character, becoming LMCT from p O to d Re. Other analogues of  $(\text{CH}_3)_3\text{ReO}_3$  were also studied by TD-DFT. The behavior of  $(\text{C}_2\text{H}_5)_3\text{ReO}_3$  is very similar, with three main absorption bands, both calculated and observed in solution. More interestingly, in both  $(\text{C}_6\text{H}_5)_3\text{ReO}_3$

and  $\{\text{C}_6\text{H}_3(\text{CH}_3)_3\}\text{ReO}_3$ , the strong low-energy absorption is dominated by a LMCT from the phenyl  $\pi^*$  to d Re ( $\pi^*$  Re–O), the calculated energy being very close to the experimental one found for  $\{\text{C}_6\text{H}_3(\text{CH}_3)_3\}\text{ReO}_3$ . The dynamics of the Re–C bond homolysis is under study and will be addressed in another publication. It is expected that the dynamical processes will involve excitation to the  $b^1A_1$  absorbing state, followed by intersystem crossing to a  $\sigma\sigma^*$  dissociative state, leading to the photoproducts.

**Acknowledgment.** P.J.C. thanks FCT for a grant (SFRH/BD/10535/2002). M.J.C., P.J.C., and C.D. gratefully acknowledge the financial support of GRICES and CNRS. This work has been undertaken as a part of a European collaborative COST project (D14/0001/99).

**Supporting Information Available:** Detailed listing of MO compositions and TD-DFT results is provided. This material is available free of charge via the Internet at <http://pubs.acs.org>.

OM0603868